JOURNAL OF SOLID STATE CHEMISTRY 71, 263–273 (1987)

Orthorhombic Superconducting $YBa_2Cu_3O_{7\pm\varepsilon}$, HREM Study

I. Structure of the Ordered Oxygen-Deficient Perovskite and Problems of Twins and Domains

M. HERVIEU, B. DOMENGÈS, C. MICHEL, J. PROVOST, AND B. RAVEAU

Laboratoire de Cristallographie et Sciences des Matériaux, ISMRa, Av. du Maréchal Juin, 14032 Caen Cedex, France

Received July 1, 1987

Study of the orthorombic high-Tc superconductor $YBa_2Cu_3O_{7\pm\varepsilon}$ was carried out by electron microscopy in an attempt to understand the influence of its non-stoichiometry on its superconducting properties. Observed and calculated high-resolution images of regular crystals of $YBa_2CU_3O_7$ were acquired in four favorable orientations. Most crystals exhibit numerous domains which can be identified as either twinning domains or oriented domains. Both phenomena are interpreted in terms of change in the orientation of the CuO_4 groups; different models are proposed. Misorientation between thin oriented domains is a typical feature, besides strains and moiré patterns.

Introduction

Following the first reports of superconductivity in the Y–Ba–Cu–O system (*1, 2*), the high-Tc superconductor $YBa_2Cu_3O_{8-y}$ was recently isolated almost simultaneously by two groups (*3, 4*). X-ray diffraction on single crystals (*5–7*) and neutron powder diffraction (*8–10*) techniques led to different conclusions. Both methods have shown that this orthorhombic oxide can be described as an ordered oxygen-deficient perovskite in which one yttrium plane alternates with two barium planes; from the neutron diffraction study, it is now clear that this structure is built up from triple layers of corner-sharing CuO_5 pyramids and CuO_4 square planar groups whose cohesion is ensured by yttrium ions (Fig. 1). The X-ray diffraction study led to a slightly different arrangement of the oxygen atoms (*5*), involving a "semi-ordered" distribution of oxygen vacancies. This different characterization can be explained by twinning of the crystals investigated by X-ray diffraction. From these results it appears that this orthorhombic superconducting phase can be formulated $YBa_2Cu_3O_{7\pm\varepsilon}$. In spite of the rather low value of ε, the deviation of the oxygen content from ideal stoichiometry may have a drastic effect on the superconducting properties of those materials. Consequently, the investigation of defects by high-resolution electron microscopy is absolutely necessary to characterize superconductivity in this oxide. A study of the HREM images of the "perfect" ordered perovskite is necessary to investigate and interpret the defects. The first part of our work deals with the study of observed and calculated HREM images and with the investigation of regular crystals of "$YBa_2Cu_3O_7$." The problem of twins and domains is also studied. The study of the

0022-4596/87 $3.00

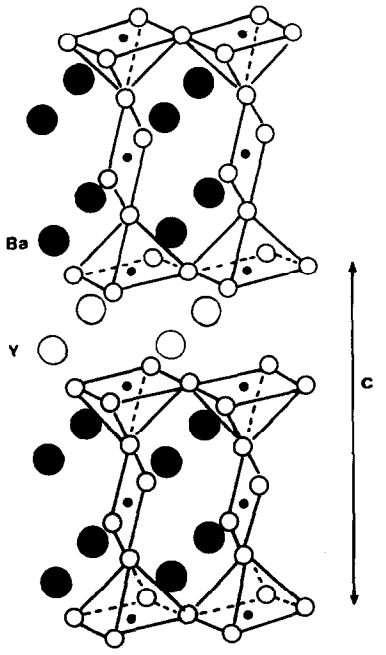

FIG. 1. Perspective view of the structure of $YBa_2Cu_3O_7$.

defects in this oxide will be the purpose of a subsequent paper.

Experimental

The orthorhombic superconducting oxide $YBa_2Cu_3O_{7\pm\varepsilon}$ was prepared according to a technique previously described (*3*): synthesis from a mixture of ultrapure oxides Y_2O_3 and CuO and barium carbonate at 1050°C in air and sintering at 950°C, followed by a slow decrease of the temperature (18°C/hr) under oxygen. The observed superconducting transition temperature was 92 K. The sample exhibits a pure orthorhombic phase with

$$a = 3.8206(1)\text{Å} \qquad b = 3.8851(1)\text{Å}$$
$$c = 11.675(4)\text{Å}$$

The material was prepared for examination in the microscope by grinding under alcohol in an agate mortar and mounted on holey carbon-coated grids. The electron diffraction study and the first investigation of sample homogeneity were carried out on a JEM 120CX fitted with a side-entry goniometer (±60°). The high-resolution electron microscopy images were recorded with a JEM 200CX, fitted with a top-entry goniometer providing a ±10° tilt about two axes. The spherical aberration constant of the objective lens was $C_s = 0.8$ mm and the objective aperture radius was 0.47 $Å^{-1}$ and 0.82 $Å^{-1}$ in reciprocal space. Astigmatism was corrected by observing the granularity of the carbon film, and micrographs were recorded at magnification in the range 550,000–710,000×. Simulated images were calculated using the multislice method and computer programs written by Skarnulis *et al.* (*11*).

Results

The reciprocal lattice of numerous crystals was constructed to test for homogeneity of the sample, thus confirming the orthorhombic symmetry, without any reflection condition, of all microcrystals. The spectacular feature of this material concerns the existence of numerous twins, domains, moiré patterns, and strains in the crystals. An HREM study is the only way to characterize these features; their detection, and particularly their interpretation, require a knowledge of the correlation between the image contrast and the structure of the material. Such an analysis is particularly necessary in the oxygen-deficient perovskites (*4–6*); indeed, the oxygen atoms contribute weakly to the image contrast whenever a slight displacement of the cations may have a noticeable effect, requiring sophisticated interpretation.

HREM Images of $YBa_2Cu_3O_7$

Four orientations of the thin crystals were chosen to study the domains: the electron beam was incident along [100], [010],

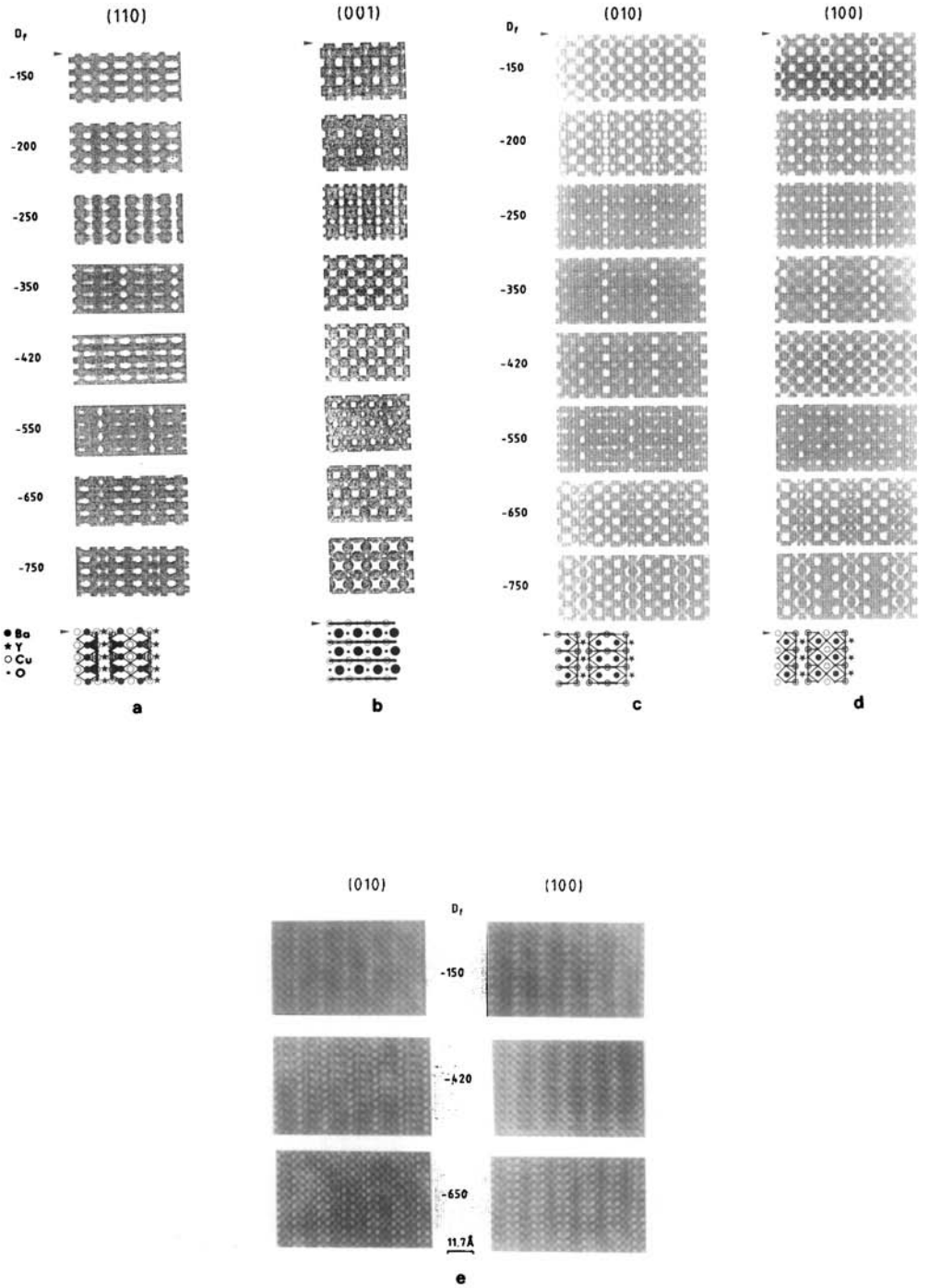

FIG. 2. Calculated through-focus series and corresponding projections of the structure. (a) [110]; (b) [001]. Large dots correspond to 2Ba + Y columns; open circles, to 3Cu + 2O; small dots, to oxygen. (c) [010]; (d) [100]; defocus specified in Å. (e) Experimental [010] and [100] images obtained for three different values of focus.

[001], or [110]. Drastic variations of the contrast were observed with changes in focus and in the thickness of the crystals. Thus, image calculations were carried out with the atomic positions obtained from the neutron diffraction study (*2*) with thicknesses 12Å $\leq t \leq$ 100Å. Small variations of oxygen content were also tried: it was confirmed that a decrease of the oxygen content from 7 to 6.9 distributed at random or in the O(4) site of the square groups does not affect the image contrast. Figure 2 shows through-focus series calculated for $YBa_2Cu_3O_7$ and with thickness of roughly 30 Å.

Clearly, the [110] orientation (Fig. 2a) does not provide the best description of the oxygen and vacancy distribution or of a possible variation in that distribution, owing to their mean projection. The [001] through-focus series (Fig. 2b), except for the −250-Å image, shows the typical perovskite contrast, characterized by two main features. First, the periodicity of the images is either 2.7 or 3.8 Å, the latter value arising from the difference between the scattering power in the Ba and Y columns (proportional to 2Ba + Y) and the Cu and O columns (proportional to 3Cu + 2O). Second, images for which low-electronic-density zones appear as light contrast (−350 Å) differ only by 2.8-Å translation from those where high-electronic-density zones are highlighted (−650 Å); this implies that the characterization of the experimental images absolutely requires that the experimental through-focus series be carried out.

Comparison of [010] and [100] through-focus series (Fig. 2c, d) points out the similarity of contrast between most of the images and proves that very few values of focus allow both orientations to be distinguished. As an example, Fig. 2e exhibits experimental images taken with both orientations and different focus values. The main difference in contrast is observed for −420 Å, as expected from the calculated images.

Twins

Electron diffraction patterns obtained from $YBa_2Cu_3O_7$ with the zone axis along the [001] direction (Fig. 3) typically exhibit split reflections, characteristic of twinned crystals: $h\bar{h}0$ reflections which are unsplit are common to both components. The relationships between the twinned domains were previously studied (*7, 12*). The angle, 2β, between the two directions $[110]^*_{\mathrm{I}}$ of one domain and $[110]^*_{\mathrm{II}}$ of an adjacent domain agrees with the theoretical value obtained from the angle between [110] and $[1\bar{1}0]$ directions of the orthorhombic cell ($90° \pm \beta$). This phenomenon results from the phase transition between the tetragonal high-temperature phase and the orthorhombic low-temperature form, at roughly 750°C (*12, 13*). By beam heating, we observed the transformation of the orthorhombic form (Figs. 4a, b) into the tetragonal form (Figs. 4c, d).

The twinning domains can readily be described by considering vacancy ordering along [010]: the change in direction of the oxygen vacancy ordering implies a perpendicular orientation of the CuO_4 groups from one domain to an adjacent one. Possible models of the junction between domains,

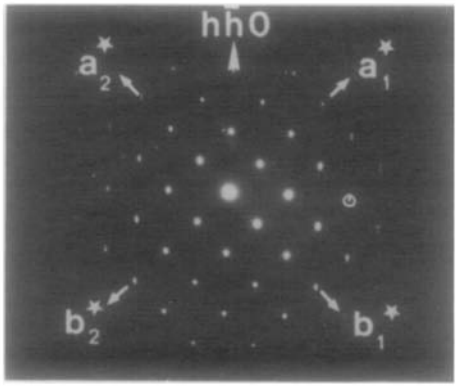

FIG. 3. Typical [001] electron diffraction pattern. Spots are split parallel to $[1\bar{1}0]^*$ except for $h\bar{h}0$ reflections. In this twinned crystal, both components are indexed.

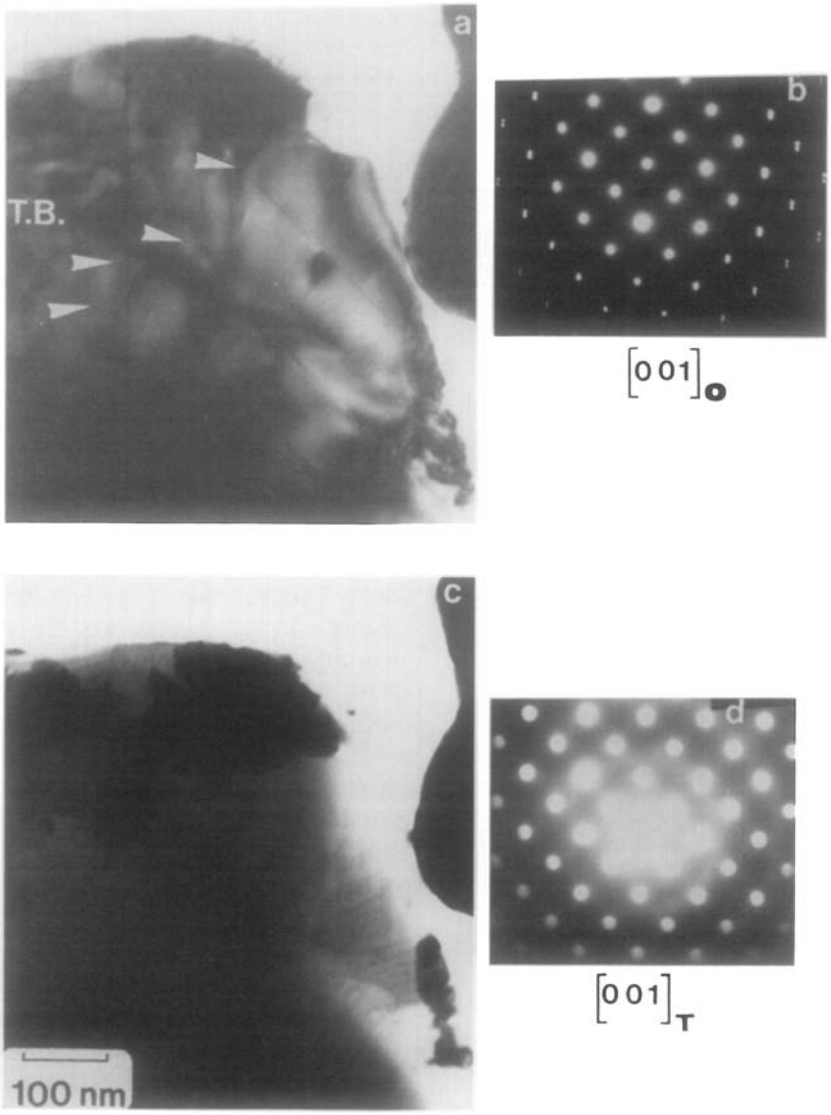

FIG. 4. (a) Low-resolution image [001] and (b) electron diffraction pattern of a typical crystal of orthorhombic $YBa_2Cu_3O_{7\pm\varepsilon}$. Twin boundaries (T.B.), which appear as black lines, are shown by arrows. (c) Low-resolution image and (d) electron diffraction pattern of the same crystal under beam heating. Note that spots are now unsplit and that the twinned domains have disappeared.

with or without (110) mirror plane, are presented in Fig. 5; only one polyhedral layer out of three is drawn to simplify the representation; we have chosen the characteristic $[CuO_2]_\infty$ layer as being built up from CuO_4 groups. The first model (Fig. 5a) with a mirror plane is based on the presence of additional CuO_6 octahedra and CuO_5 pyramids in the $[CuO_2]_\infty$ layer at the boundary. In the second model, the junction is achieved solely by CuO_5 pyramids, as shown in Fig. 5b. These two models imply the presence of additional oxygen at the boundary but no drastic displacements in

the cation framework. A third model, the simplest because the junctions are achieved solely through tetrahedra, can also be constructed. However, the existence of such CuO_4 tetrahedra, which involves a displacement of the Cu atoms, appears to be really less favorable (Fig. 5c). The dark-field image (Fig. 6a) obtained by selecting a reflection 220 (circled in Fig. 3) with the objective aperture permits the domains to be displayed and their width to be measured; it appears that from one crystal to the other the domain width is variable but its mean value ranges from 500 to 1000 Å.

The equivalence of the [110] and [1$\bar{1}$0] directions is illustrated in Fig. 6b by the simultaneous existence of quasi-perpendicular twinning domains in the thicker crystals. The idealized model (Fig. 6c) shows the arrangement of the $[CuO_2]_\infty$ planes at the quasi-perpendicular boundaries. Such a phenomenon can easily take place because the domains result from a change in vacancy ordering within the core of the matrix without any large displacement of the cations in the host lattice.

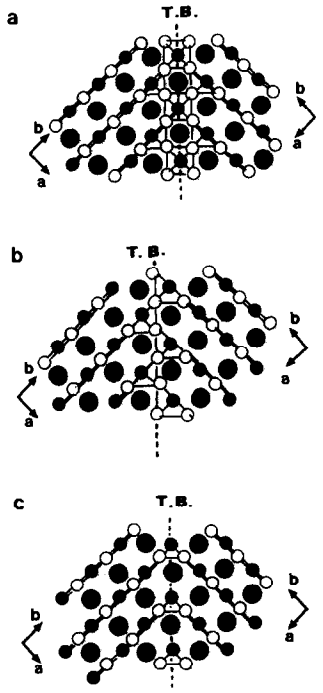

FIG. 5. Three idealized models of junctions between the twinning domains in the $[CuO_2]_\infty$ layers. (a) Junction in a mirror plane through CuO_6 octahedra and CuO_5 pyramids. (b) Junction through CuO_5 pyramids and (c) junction in a mirror plane through CuO_4 tetrahedra. Note that in contrast with the third model the first two imply additional oxygen; such arrangements between octahedra and pyramids are frequently observed in oxygen-deficient perovskites.

Through such twin boundaries, the O–Cu–O chains are not actually broken but zigzag in the $[CuO_2]_\infty$ layer of the perovskite matrix. As previously shown (Figs. 5a, b), such a change in the O–Cu–O chains requires the presence of additional oxygen; moreover, the problem of the existence of defects resulting from these junctions between two adjacent twinning domains can be considered. To check this feature, the best orientations are indeed [110] and [001], owing to their direction with regard to the twin plane. Observations of the twinned crystals along [110] do not provide any important structural information (owing to a mean projection of the oxygen atoms, as shown from the calculated images) but they clearly show that no particular defect areas are coupled with the domain boundaries. With an aperture of 0.85 $Å^{-1}$, the micrographs recorded along [001] from a well-oriented crystal show a similar contrast from one domain to the other, which thus are hardly distinguishable. It is necessary to use a smaller objective aperture (0.48 $Å^{-1}$) to make the domain boundaries appear, and this only in that part of the bulk where black lines image them (Fig. 7a). An enlargement of the thin part of the crystal (Fig. 7b) close to a twin boundary (T.B.) shows the presence of numerous defects which are not localized specifically at the boundary areas but within the whole matrix (*14–15*).

Two other orientations, [010] and [100], are theoretically favorable for the observation of changes in direction of the CuO_4

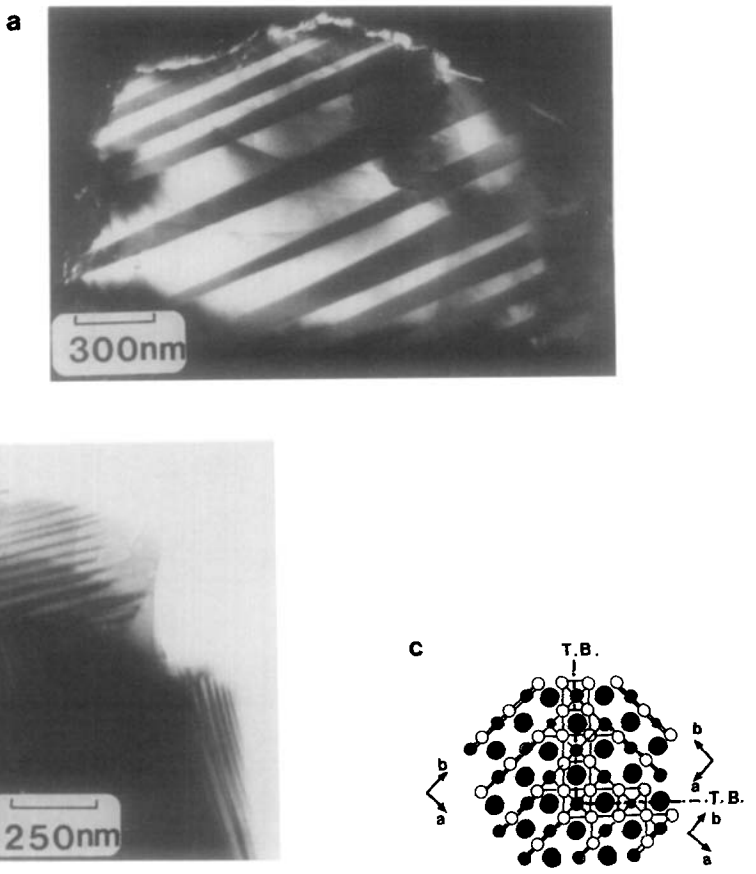

FIG. 6. (a) Dark-field image [001] of twinned domains. The selected reflection is circled in Fig. 3. (b) Low-resolution image of quasi-perpendicular twinned domains. (c) idealized model showing the arrangement of the $[CuO_2]_\infty$ planes in the quasi-perpendicular boundaries.

groups, since they can be distinguished through characteristic variations in contrast for some particular values of the focus. However, the 45° orientation of the domain boundary with respect to the *a* and *b* axes implies an overlap of the two adjacent domains whose width is equal to the crystal thickness. Such an overlap obviously affects the contrast and hinders the detection of defects in the close neighborhood of the boundary.

Oriented Domains

The observation of the $YBa_2Cu_3O_7$ crystals in such orientations showed that a second type of domain exists which forms slices perpendicular to the *c* axis (Fig. 8). Such domains can more easily be interpreted for crystals with a *c* axis parallel to the thin edge (Fig. 9a). Enlargements of areas labeled 1 and 2 are shown: area 1 exhibits the typical contrast of a [100] image for $t \approx 30$ Å and $D_f \approx -430$ Å, whereas area 2 is characteristic of a [010] image, under the same conditions. Such domains are interpreted by invoking a change in orientation of the $[CuO_2]_\infty$ layers, from one triple polyhedral layer to the adjacent one, forming "oriented" slices perpendicular to the *c* axis; the idealized model of the "oriented" domains is proposed in Fig. 9b. It is worth pointing out that, in contrast to

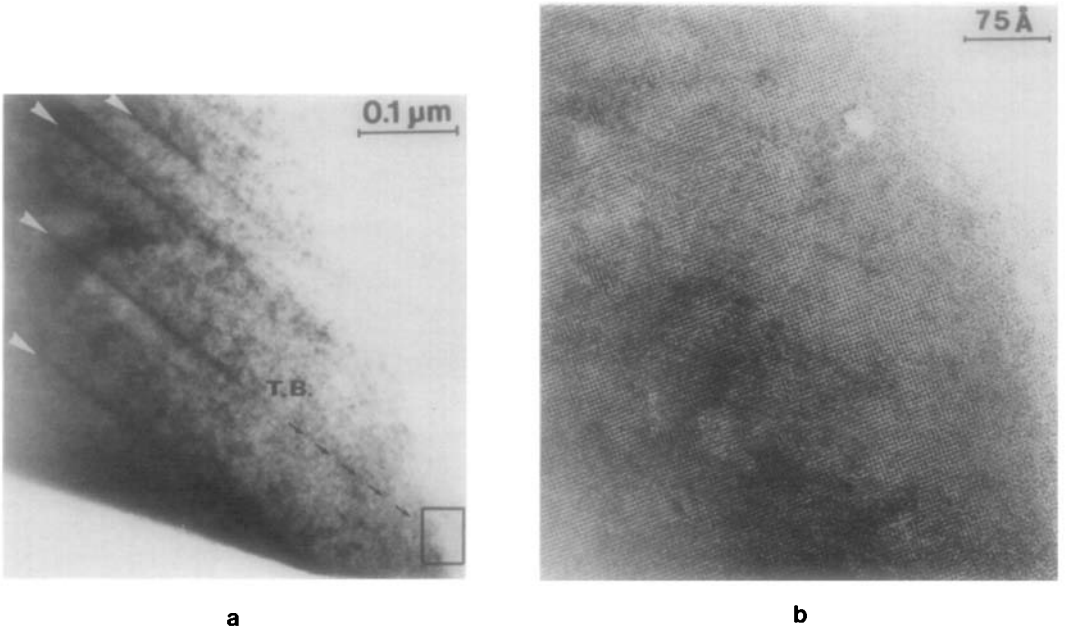

FIG. 7. (a) [001] image showing in the thick part of the crystal twin boundaries (black lines shown by arrows). (b) Enlargement of a twin boundary (T.B.) in the edge of the crystal; defects appear all over the matrix instead of close to the T.B.

the twinning domains, these domains are characterized by a junction involving a juxtaposition of two different parameters a and b, respectively at the boundary. The domain interfaces are then particularly disturbed, as observed in the thicker part of the bulk.

Misorientations of Crystal Areas

Another typical structural feature corresponds to misorientation of crystal areas. A characteristic diffraction pattern of such crystals is shown in Fig. 10. We clearly observed the contribution of every compo-

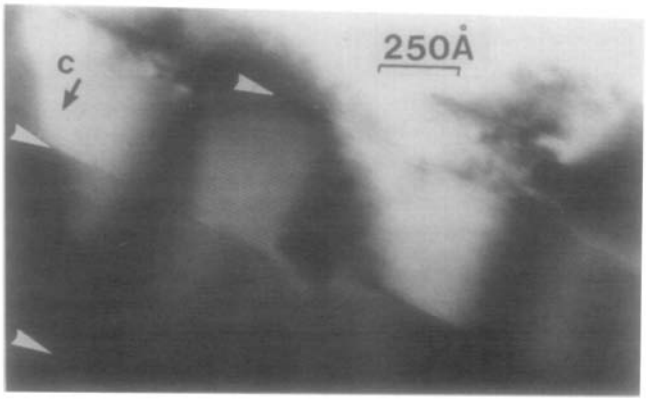

FIG. 8. Medium-resolution image of a crystal where domains form slices perpendicular to the c axis (arrowhead).

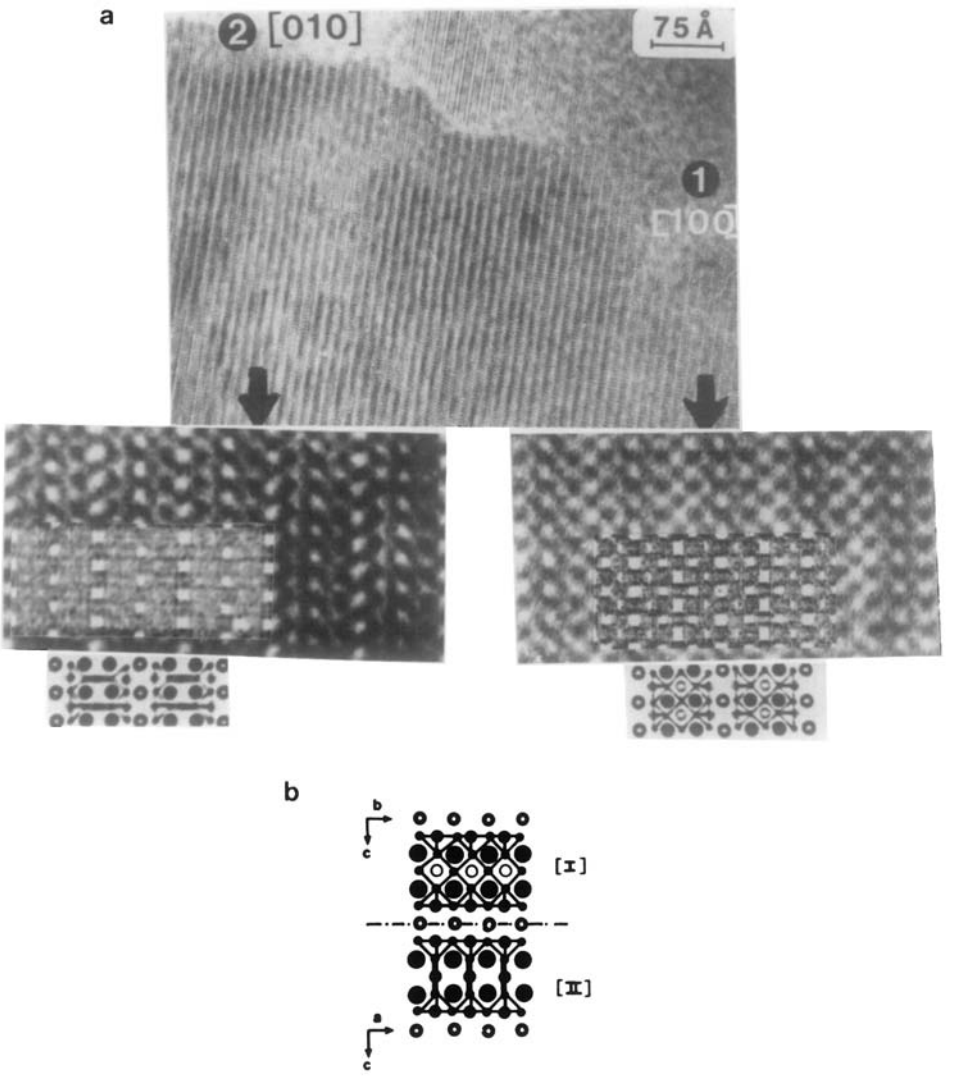

FIG. 9. (a) High-resolution image of "oriented" domains; areas labeled 1 and 2, respectively, show contrast corresponding to [100] and [010] images; calculated images enclosed in the enlargements were calculated for a defocus of −430 Å and thickness of ~30 Å. (b) Idealized model of these oriented domains.

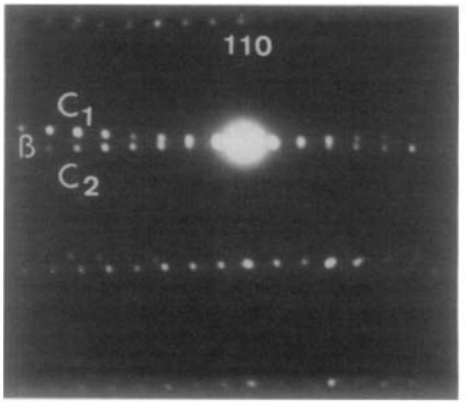

FIG. 10. Typical diffraction pattern of a crystal with misoriented areas; the two c axes differ by an angle β.

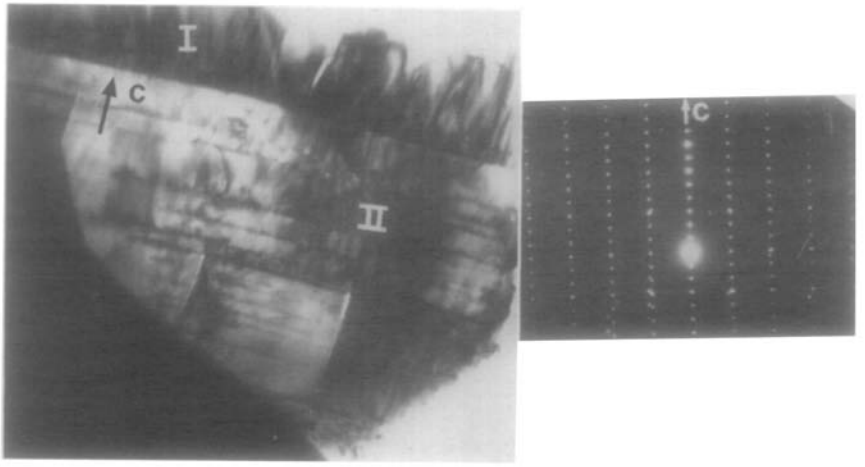

FIG. 11. Low-resolution image of most common crystals and corresponding diffraction pattern; both twinned (*I*) and oriented (*II*) domains are observed.

nent to the pattern. However, the β angle between the domains varies from one crystal to the next. It appears that the majority of the corresponding crystals exhibit the two types of domains (Fig. 11): domains of the first type, the twinning domains, are ob-

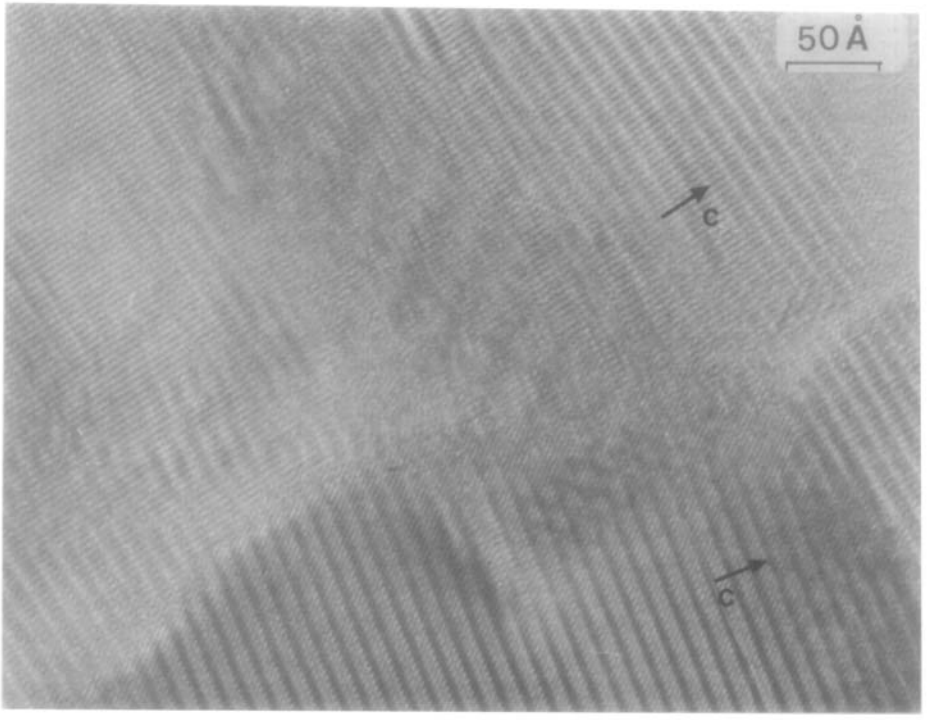

FIG. 12. High-resolution image of a crystal showing overlap of misoriented domains; strains related to microfractures and moiré patterns are observed.

served in the area labeled I and domains of the second type, oriented domains, are observed in the crystal perpendicular to $\vec{c}$ (labeled II). When the domains are numerous and thin, as in this case, the discrepancy between parameters (≈2%) results in spectacular strains and bending of the crystal. From those observations, we assume that the strains are reduced by loosening the framework through the mechanism of microfractures; they just begin to form at the edge of the crystals but are not always achieved. The overlapping of two adjacent domains leads sometimes to moiré patterns; such microfractures explain the variations of the β angles. An HREM image of such a misorientation is shown in Fig. 12. The angle between two domains and their overlaps are clearly visible.

Conclusion

From this work, it appears that a large majority of the microcrystals of the superconductor $YBa_2Cu_3O_7$ exhibit numerous domains which result from change in the direction of the CuO_4 groups within one triple layer or from one triple layer to the other. Twinning domains involve additional oxygens in the boundaries and the multiplicity of such domains is a favorable factor in achieving an overstoichiometry of oxygen, thereby producing the superconducting properties. By contrast, oriented domains perpendicular to the *c* axis produce strains in the crystals, owing to a mismatch of the parameters at the interface; this results in misorientations which could affect those properties, by layer and O–Cu–O chain breaking.

References

1. *People's Daily* (China), Feb. 25, 1987.
2. M. K. Wu, J. R. Ashburn, C. J. Torng, P. H. Hor, R. L. Meng, L. Gao, Z. J. Huang, Y. Q. Wang, and C. W. Chu, *Phys. Rev. Lett.* **58,** 908 (1987).
3. C. Michel, F. Deslandes, J. Provost, P. Lejay, R. Tournier, M. Hervieu, and B. Raveau. *C.R. Acad. Sci. Ser. 2* **304**(17), 1050 (1987).
4. R. J. Cava, B. Battlog, R. B. van Dover, D. W. Murphy, S. Sunshine, T. Siegrist, J. P. Remeika, E. A. Rietman, S. Zahurak and G. P. Espinosa, *Phys. Rev. Lett.* **58,** 1676 (1987).
5. Y. Lepage, W. R. McKinnon, J. M. Tarascon, L. H. Greene, G. W. Hull, and D. M. Hwang, *Phys. Rev.* **B35,** 7245 (1987).
6. T. Siegrist, S. Sunshine, D. W. Murphy, R. J. Cava and S. M. Zahurak, American Physics Society Meeting, New York, March 1987.
7. G. Roth, D. Ewert, G. Heger, C. Michel, M. Hervieu, B. Raveau, F. d'Yvoire, and A. Revcolevschi, *Z. Phys.*, in press.
8. J. J. Capponi, C. Chaillout, A. W. Hewat, P. Lejay, M. Marezio, N. Nguyen, B. Raveau, J. L. Soubeyroux, J. L. Tholence, and R. Tournier, *Europhys. Lett.* **12,** 1301 (1987).
9. L. Sonderholm *et al.*, 2nd International Conference on the Chemistry and Technology of Lanthanides and Actinides, Lisbon, April 8, 1987.
10. B. Raveau, 2nd International Conference on the Chemistry and Technology of Lanthanides and Actinides, Lisbon, April 8, 1987.
11. A. J. Skarnulis, E. Summerville, and L. Eyring, *J. Solid State Chem.* **23,** 59 (1987).
12. M. Hervieu, B. Domengès, C. Michel, G. Heger, J. Provost, and B. Raveau, *Phys. Rev. Lett.*, in press.
13. I. K. Schuller, D. G. Hinks, M. A. Beno, D. W. Capone II, L. Soderholm, J. P. Locquet, Y. Bruynseraede, C. H. Segre, and Z. Zang, *Solid State Commun.*, submitted for publication.
14. M. Hervieu, B Domengès, C. Michel, and B. Raveau, *Europhys. Lett.* **6,** 205 (1987).
15. B. Domengès, M. Hervieu, C. Michel, and B. Raveau, *Europhys. Lett.* **6,** 211 (1987).